*J. Fluid Mech.* (1995), *vol.* 298, *pp.* 327–339
Copyright © 1995 Cambridge University Press


# Oscillatory internal shear layers in rotating and precessing flows

By R. HOLLERBACH[1] AND R. R. KERSWELL[2]

[1] Institute of Geophysics and Planetary Physics, Los Alamos National Laboratory, Los Alamos, NM 87545, USA

[2] Department of Mathematics and Statistics, University of Newcastle upon Tyne, Newcastle NE1 7RU, UK

(Received 21 July 1994 and in revised form 6 April 1995)

We present a direct numerical solution of a particular inertial oscillation, the so-called 'spin-over' mode, in spherical geometry. This mode is particularly relevant to the fluid flow within a precessing oblate spheroid. We demonstrate that the oscillatory Ekman layer breaks down at $\pm 30°$ latitude, and that this breakdown spawns internal shear layers. We show that the structure of these shear layers is different for a full sphere and a spherical shell, as noted in the preceding paper (Kerswell 1995). Despite the existence of these shear layers, however, the numerical decay rates agree to within 1 % with the asymptotic decay rates, which neglect any possible shear layers. Finally, we consider the nonlinear mean flow profiles driven by this mode, and demonstrate that our numerical results agree reasonably well with experimental results.

## 1. Introduction

It is well known that rotating fluid systems will support inertial oscillations. In particular, the steady precession of a rotating fluid-filled oblate spheroid maintains at a constant amplitude one particular inertial oscillation, the so-called spin-over mode, consisting of a rotation about an axis other than the rotation axis of the container (Poincaré 1910). In this work we consider this spin-over mode in spherical geometry, in order to most easily identify the associated viscous flows generated. In the study of rotating precessing flows, a spherical container presents a particular difficulty, because the precessional motion of the container can only be transmitted to the fluid by viscous forces, which are assumed to be small. For this reason, instead of the precessionally forced spin-over mode, we consider the unforced spin-over mode. As noted by Greenspan (1968, p. 67), 'Precession may be viewed as a sequence of infinitesimal changes [in the axis of rotation] and it is anticipated that this mode will play a key role in that problem'.

To demonstrate the similarity between the precessionally forced mode and the unforced mode, we begin by considering the equation of motion in a rotating and precessing reference frame,

$$\frac{\partial}{\partial t}\boldsymbol{v}+(\boldsymbol{v}\cdot\nabla)\boldsymbol{v}+2(\hat{\boldsymbol{k}}+\boldsymbol{\Omega})\times\boldsymbol{v}=-\nabla p+E\nabla^2\boldsymbol{v}+(\hat{\boldsymbol{k}}\times\boldsymbol{\Omega})\times\boldsymbol{r}, \tag{1.1}$$

where $\hat{\boldsymbol{k}}+\boldsymbol{\Omega}$ is the *total* rotation rate, consisting of the basic rotation $\hat{\boldsymbol{k}}$ plus the precession $\boldsymbol{\Omega}$ of that basic rotation. The effect of the precession is thus to introduce the so-called Poincaré force $(\hat{\boldsymbol{k}}\times\boldsymbol{\Omega})\times\boldsymbol{r}$ (Malkus 1968).

In a spheroid of oblateness $\eta$, an *exact* solution to this equation of motion (1.1) is Poincaré's (1910) inertial spin-over mode

$$v_z = \epsilon s \sin(\phi + t), \quad v_s = -\epsilon(1+\eta) z \sin(\phi + t), \quad v_\phi = -\epsilon(1+\eta) z \cos(\phi + t), \quad (1.2)$$

in which the fluid's rotation axis is merely displaced slightly from the container's rotation axis. The amplitude $\epsilon$ is given in terms of the oblateness $\eta$ and the precession rate $\boldsymbol{\Omega}$. The structure and stability of this solution have been discussed in considerably more detail by Kerswell (1993).

The point we wish to focus on in this work is that this spin-over mode does not, of course, satisfy the no-slip boundary conditions, and so there will be viscous Ekman boundary layers. Roberts & Stewartson (1963) have demonstrated that these oscillatory Ekman layers break down at a certain critical latitude. The effect of this breakdown on the interior flow has thus long been an issue of some concern. Quoting Greenspan (1968, p. 62) once again: 'The likely effect of the critical zones might be to establish weak internal shear layers along the characteristic direction'. The preceding paper (Kerswell 1995, hereafter referred to as I) has presented arguments to support this view. In this paper, we provide direct numerical evidence to confirm that internal shear layers are indeed present, and that their structure appears consistent with the scalings discussed in I.

For numerical reasons, it is easier to work in spherical, rather than spheroidal, geometry. However, as noted above, spherical geometry presents a particular difficulty, because the precessional motion of the container can only be transmitted to the fluid by the small viscous forces. For this reason, instead of the precessionally forced momentum equation (1.1), we consider the unforced momentum equation

$$\frac{\partial}{\partial t}\boldsymbol{v} + (\boldsymbol{v}\cdot\boldsymbol{\nabla})\boldsymbol{v} + 2\hat{\boldsymbol{k}}\times\boldsymbol{v} = -\boldsymbol{\nabla}p + E\nabla^2\boldsymbol{v}. \quad (1.3)$$

We expand the velocity field in the Rossby number $\epsilon$, which is typically small,

$$\boldsymbol{v} = \epsilon\boldsymbol{u}_0 + \epsilon^2\boldsymbol{u}_1 + \ldots, \quad (1.4)$$

computing numerically the linear term $\boldsymbol{u}_0$ and then using this to calculate the axisymmetric part of the nonlinear term $\boldsymbol{u}_1$.

This equation of motion (1.3) will also support an inertial spin-over mode. Experimentally, this mode would be generated by impulsively tipping the rotation axis of the spherical container. The resulting disturbance would then be the slowly decaying spin-over mode we consider here. In the reference frame rotating with the spherical container, an inviscid spin-over mode, that is a solid-body rotation about an axis different from the rotation axis of the container, would be represented by (Greenspan 1968)

$$v_z = \epsilon s \sin(\phi + t), \quad v_s = -\epsilon z \sin(\phi + t), \quad v_\phi = -\epsilon z \cos(\phi + t), \quad (1.5)$$

or, alternatively, in spherical coordinates,

$$v_r = 0, \quad v_\theta = -\epsilon r \sin(\phi + t), \quad v_\phi = -\epsilon r \cos\theta \cos(\phi + t). \quad (1.6)$$

It is this similarity between the precessionally forced spheroidal spin-over mode (1.2) and the unforced spherical spin-over mode (1.5) that motivates this work. The internal shear layers one then obtains in spherical geometry are likely to be very similar to the shear layers one would obtain in spheroidal geometry. The biggest difference is probably that we are no longer maintaining the flow at any definite amplitude $\epsilon$. Indeed, it must be noted that our results are valid only in the weakly nonlinear regime,

whereas the experiments are typically done in the more strongly nonlinear regime. This difference is probably as important as the slight geometrical differences.

In this paper we present a direct numerical solution of the viscous spin-over mode in spherical geometry, for Ekman numbers as small as $E = 10^{-6}$, explicitly resolving all boundary and internal layers that may develop. From (1.3) and (1.4), the equation governing the linear spin-over mode is

$$\frac{\partial}{\partial t}\boldsymbol{u}_0 + 2\hat{\boldsymbol{k}} \times \boldsymbol{u}_0 = -\nabla p + E\nabla^2 \boldsymbol{u}_0, \tag{1.7}$$

where we are interested in the particular time-dependence $\partial/\partial t \equiv \mathrm{i}(1+\lambda)$. That is, we are interested in this one particular free inertial oscillation having a frequency of essentially 1. The complex eigenvalue $\lambda$ is then the (small) viscous correction to the inviscid spin-over frequency of 1, and is to be determined as part of the solution. In §2 we present a direct numerical solution of the resulting linear eigenvalue problem, both in a full sphere and in a spherical shell.

We demonstrate that the oscillatory Ekman layer does indeed break down, at a latitude of 30° for this particular frequency, and that this breakdown does spawn internal shear layers, as suggested by Greenspan (1968). Furthermore, as discussed in I, we show that the structure of these shear layers is indeed different for the full sphere and the spherical shell. In the full sphere there is only one characteristic direction that the shear layers can propagate along, whereas in the spherical shell there are three: one tangential to the inner Ekman layer eruption, and one non-tangential to each of the inner and outer Ekman layer eruptions, as in figure 1 of I. The Ekman layers are known to break down over an $O(E^{1/5})$ range. The non-tangential shear layers will thus see a generating region of width $O(E^{1/5})$, whereas the tangential shear layer will see a generating region of width $O(E^{2/5})$. As demonstrated by Walton (1975), the 'natural' width of such shear layers is $O(E^{1/3})$. Thus, the non-tangential shear layers see a generating region thicker than their 'natural' width, whereas the tangential shear layer sees a generating region thinner than its 'natural' width. The result is that the full sphere shear layer adjusts to the $O(E^{1/5})$ scaling, whereas the spherical shell shear layer remains at the $O(E^{1/3})$ scaling, as noted in I. While we are not able to reach sufficiently small Ekman numbers to precisely confirm these scalings, we are able to demonstrate that the scalings are different, and not inconsistent with the asymptotic scalings noted above. Section 3 presents the linear eigenmodes in the sphere and the spherical shell, demonstrating the differences in the structures of the shear layers.

Finally, we consider the nonlinear mean flow profiles driven by the self-interaction of the linear spin-over mode. From (1.3) and (1.4), the solutions $\boldsymbol{u}_0$ of (1.7) will induce the nonlinear response

$$\frac{\partial}{\partial t}\boldsymbol{u}_1 + 2\hat{\boldsymbol{k}} \times \boldsymbol{u}_1 = -\nabla p + E\nabla^2 \boldsymbol{u}_1 - (\boldsymbol{u}_0 \cdot \nabla)\boldsymbol{u}_0. \tag{1.8}$$

In §4 we present a direct numerical solution of the axisymmetric portion of (1.8), again both in the full sphere and in the spherical shell. Section 5 presents the nonlinear responses, and compares them with the experiments of Malkus (1968) and Vanyo *et al.* (1995).

## 2. Numerical solution of the linear problem

As in Hollerbach (1994*a*), we begin by decomposing:

$$\boldsymbol{u}_0 = \nabla \times (e\hat{\boldsymbol{r}}) + \nabla \times \nabla \times (f\hat{\boldsymbol{r}}), \tag{2.1}$$

thereby satisfying the incompressibility condition $\nabla \cdot \boldsymbol{u}_0 = 0$. We then expand $e$ and $f$ as

$$e(r,\theta,\phi) = \sum_{n=1}^{N_1} e_n(r)\, P_{n_1}^{(1)}(\cos\theta) \exp[\mathrm{i}\phi + \mathrm{i}(1+\lambda)\, t], \tag{2.2a}$$

$$f(r,\theta,\phi) = \sum_{n=1}^{N_1} f_n(r)\, P_{n_2}^{(1)}(\cos\theta) \exp[\mathrm{i}\phi + \mathrm{i}(1+\lambda)\, t], \tag{2.2b}$$

where $P_n^{(1)}(\cos\theta)$ are associated Legendre functions, with $n_1 = 2n-1$ and $n_2 = 2n$. Note that we have thereby chosen a particular symmetry about the equator. This symmetry, as well as the azimuthal dependence $\exp(\mathrm{i}\phi)$, is chosen to agree with the inviscid mode (1.6). The viscous mode we are interested in will differ in many respects from the inviscid mode, but it will exhibit the same equatorial symmetry and azimuthal wavenumber.

Having expanded as (2.2), the $r$-components of the curl and the curl of the curl of (1.7) yield

$$\begin{aligned}
&\sum_{n=1}^{N_1} [n_1(n_1+1)\,\mathrm{i} - 2\mathrm{i} - E n_1(n_1+1)\, L_{n_1}] \frac{e_n}{r^2} P_{n_1}^{(1)}(\cos\theta) \\
&\quad + \sum_{n=1}^{N_1} \frac{2}{r^2}\left[\frac{n_2(n_2+1)}{r} - \frac{\mathrm{d}}{\mathrm{d}r}\right] f_n \sin\theta \frac{\mathrm{d}}{\mathrm{d}\theta} P_{n_2}^{(1)}(\cos\theta) \\
&\quad + \sum_{n=1}^{N_1} \frac{2}{r^2} n_2(n_2+1)\left[\frac{2}{r} - \frac{\mathrm{d}}{\mathrm{d}r}\right] f_n \cos\theta P_{n_2}^{(1)}(\cos\theta) \\
&= -\lambda \sum_{n=1}^{N_1} n_1(n_1+1)\,\mathrm{i} \frac{e_n}{r^2} P_{n_1}^{(1)}(\cos\theta),
\end{aligned} \tag{2.3a}$$

$$\begin{aligned}
&\sum_{n=1}^{N_1} [n_2(n_2+1)\,\mathrm{i} - 2\mathrm{i} - E n_2(n_2+1)\, L_{n_2}] L_{n_2} \frac{f_n}{r^2} P_{n_2}^{(1)}(\cos\theta) \\
&\quad - \sum_{n=1}^{N_1} \frac{2}{r^2}\left[\frac{n_1(n_1+1)}{r} - \frac{\mathrm{d}}{\mathrm{d}r}\right] e_n \sin\theta \frac{\mathrm{d}}{\mathrm{d}\theta} P_{n_1}^{(1)}(\cos\theta) \\
&\quad - \sum_{n=1}^{N_1} \frac{2}{r^2} n_1(n_1+1)\left[\frac{2}{r} - \frac{\mathrm{d}}{\mathrm{d}r}\right] e_n \cos\theta P_{n_1}^{(1)}(\cos\theta) \\
&= -\lambda \sum_{n=1}^{N_1} n_2(n_2+1)\,\mathrm{i} L_{n_2} \frac{f_n}{r^2} P_{n_2}^{(1)}(\cos\theta),
\end{aligned} \tag{2.3b}$$

where the operator

$$L_n = \frac{1}{r^2}\frac{\mathrm{d}^2}{\mathrm{d}r^2} r^2 - \frac{n(n+1)}{r^2}. \tag{2.4}$$

By applying the appropriate recursion relations (Abramowitz & Stegun 1968), one can show that $\sin\theta\,(\mathrm{d}/\mathrm{d}\theta)\, P_n^{(1)}(\cos\theta)$ and $\cos\theta P_n^{(1)}(\cos\theta)$ are both linear combinations only of $P_{n\pm1}^{(1)}(\cos\theta)$. Thus, explicitly separating out the angular dependence, (2.3$a$) couples $e_n$ only to $f_{n-1}$ and $f_n$, and (2.3$b$) couples $f_n$ only to $e_n$ and $e_{n+1}$.

Arranging these as in figure 1 results in the complex matrix eigenvalue problem

$$\boldsymbol{A}\boldsymbol{v} = \lambda \boldsymbol{B}\boldsymbol{v}, \tag{2.5}$$

where $\boldsymbol{A}$ is block tri-diagonal and $\boldsymbol{B}$ is block diagonal. Each block of course still contains the radial structure, discussed below. The banded structure of these matrices $\boldsymbol{A}$ and $\boldsymbol{B}$ will turn out to be crucial: in order to resolve the various boundary and

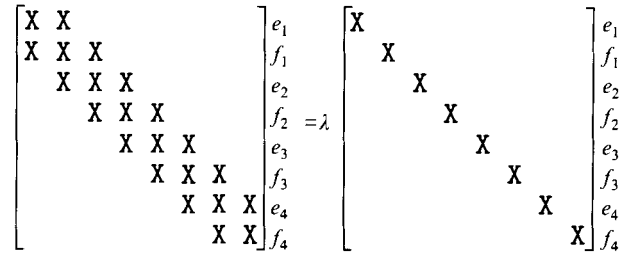


FIGURE 1. A schematic diagram of the banded matrix eigenvalue problem (2.5) that results when (2.3) are arranged as shown. Each block still contains the details of the radial expansion.

internal layers for Ekman numbers as small as $E = 10^{-6}$, one needs a very high truncation. The dimension of $\boldsymbol{A}$ and $\boldsymbol{B}$ is then so large ($2N_1 M_1 = 20000$) that one could not even store them, were they not banded. However, as they are banded, 256 Mbytes of computer memory is more than sufficient for the entire calculation.

Turning briefly now to the implementation of the radial structure, we expand $e_n$ and $f_n$ in terms of Chebyshev polynomials, collocated at $M_1$ collocation points, essentially as in Hollerbach (1994*a*), except that we now impose the no-slip boundary conditions

$$f_n = \frac{\mathrm{d}}{\mathrm{d}r} f_n = e_n = 0. \tag{2.6}$$

The implementation of the boundary conditions within each diagonal block of $\boldsymbol{A}$ is as in Hollerbach (1994*b*). The precise details of the radial expansion will not be presented here, as they are rather tedious, and immaterial to the further discussion. Also, there are a few subtle differences between the full sphere and the spherical shell expansions.

To solve the eigenvalue problem (2.5), we use inverse iteration (Peters & Wilkinson 1971)

$$\boldsymbol{v}^{(m)} = \boldsymbol{A}^{-1}\boldsymbol{B}\boldsymbol{v}^{(m-1)}. \tag{2.7}$$

Fearn (1991) has provided a very nice one-dimensional example of the power of this method in solving for boundary-layered eigensolutions; we provide a two-dimensional example here. We begin with one call to the NAG routine F01NAF to obtain the LU decomposition of $\boldsymbol{A}$, followed by repeated calls to F04NAF to obtain successive iterates of (2.7). Successive iterates will then converge rather rapidly to the eigenvector having the smallest $|\lambda|$. It is known (Greenspan 1964) that $|\lambda|$ scales asymptotically as $O(E^{1/2})$, and so the iteration will indeed converge to the desired eigenvector. The iteration converges in the sense that successive iterates become (complex) multiples of one another, and the multiplicative factor is then precisely $\lambda^{-1}$:

$$\boldsymbol{v}^{(m)} = \lambda^{-1}\boldsymbol{v}^{(m-1)}, \tag{2.8}$$

after a dozen or so iterations. Also, since most of the computational effort goes into the LU decomposition of $\boldsymbol{A}$, once that is accomplished one might as well do enough iterations to obtain convergence to full machine precision.

## 3. Linear results

### 3.1. *Full sphere*

We begin by considering the dependence of the eigenvalue $\lambda$ on the Ekman number $E$. Table 1 shows the quantity $\mathrm{i}\lambda/E^{1/2}$ as a function of $E$, from $10^{-4.5}$ to $10^{-6.5}$. According to Greenspan's boundary layer analysis, in the asymptotic limit this quantity should be

$$\mathrm{i}\lambda/E^{1/2} = -2.620 + 0.259\mathrm{i}.$$

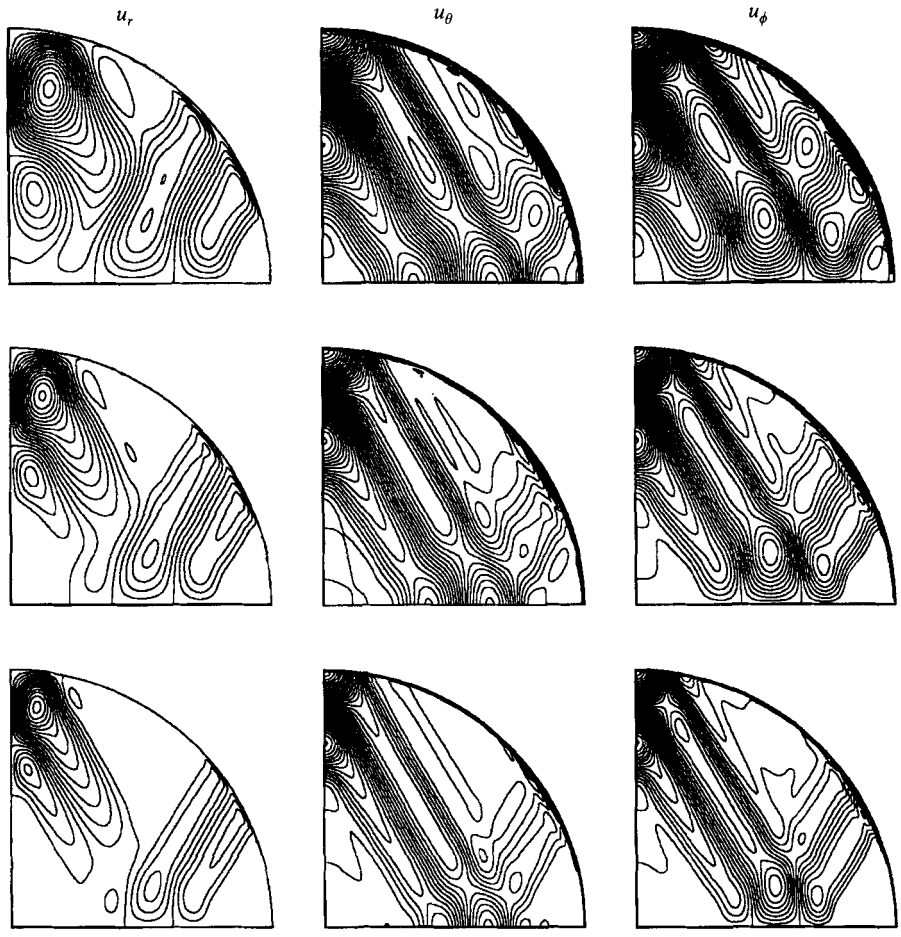


FIGURE 2. The structure of the full-sphere eigenmodes $\boldsymbol{u}_0$. From top to bottom $E = 10^{-5}$, $10^{-5.5}$, $10^{-6}$. Contour intervals of 0.01.

| $E$ | $i\lambda/E^{1/2}$ |
|---|---|
| $10^{-4.5}$ | $-2.706+0.396i$ |
| $10^{-5}$ | $-2.679+0.377i$ |
| $10^{-5.5}$ | $-2.662+0.353i$ |
| $10^{-6}$ | $-2.651+0.330i$ |
| $10^{-6.5}$ | $-2.644+0.312i$ |

TABLE 1. The dependence of the eigenvalue $\lambda$ on $E$ for the full sphere. The asymptotic limit is $i\lambda/E^{1/2} = -2.620+0.259i$.

The asymptotic decay factor is thus in excellent agreement with the numerical values obtained here. (Greenspan 1968, p. 66, also quotes an experimental decay factor of $-2.82E^{1/2}$, as determined by Malkus.) The agreement in the asymptotic frequency correction is not quite so good. However, it should be noted in table 1 that the relative variation of the frequency corrections is considerably greater than the relative variation of the decay factors. Presumably the asymptotic limit of the frequency correction is only reached at even smaller Ekman numbers. Perhaps the internal shear layers,

| $E$ | $i\lambda/E^{1/2}$ |
|---|---|
| $10^{-4}$ | $-1.860+0.239i$ |
| $10^{-4.5}$ | $-1.831+0.242i$ |
| $10^{-5}$ | $-1.813+0.231i$ |
| $10^{-5.5}$ | $-1.799+0.222i$ |
| $10^{-6}$ | $-1.793+0.212i$ |

TABLE 2. The dependence of the eigenvalue $\lambda$ on $E$ for the spherical shell. The asymptotic limit is $i\lambda/E^{1/2} = -1.776+0.176i$.

neglected in Greenspan's analysis, have a relatively strong effect on the frequency correction.

Turning now to the structure of the eigenmodes, figure 2 shows the solutions at $E = 10^{-5}$, $10^{-5.5}$, and $10^{-6}$. The arbitrary amplitude has been normalized so that the total angular momentum of the solution is the same as that of a solid-body rotation of angular velocity unity, as in the inviscid mode (1.6). This solid-body rotation has then been subtracted out in figure 2, to focus exclusively on the viscous corrections to the inviscid mode. The particular meridional sections shown have been chosen to emphasize the structure of the shear layers: $u_r$ and $u_\theta$ are in phase, and $u_\phi$ is 90° out of phase. One notes very clearly the breakdown of the Ekman layer at 30° latitude, and the internal shear layers, inclined at exactly 30° to the container's axis of rotation, spawned thereby.

Verifying the asymptotic scalings derived in I is rather difficult, primarily because it is unclear how to define an objective quantifiable measure of the width of the shear layers. However, it is quite clear that the Ekman layer breaks down over a rather broad range in latitude, and that the shear layers are spawned over this entire range. Their precise width is certainly not inconsistent with an $O(E^{1/5})$ scaling: this would imply that between $E = 10^{-5}$ and $10^{-6}$ the shear layers should become thinner by a factor of $10^{1/5} = 1.6$, which is essentially as observed. Furthermore, it is equally clear that the flow within the shear layers decreases with decreasing Ekman number. The precise magnitude is again not inconsistent with an $O(E^{3/10})$ scaling. For example, the number of contour lines in the most clearly defined shear layer in $u_\theta$ is 12 for $E = 10^{-5}$, but only 6 for $E = 10^{-6}$, in agreement with $10^{3/10} = 2$.

### 3.2. *Spherical shell*

We again begin by considering the dependence of the eigenvalue $\lambda$ on $E$. Table 2 shows the quantity $i\lambda/E^{1/2}$ as a function of $E$, from $10^{-4}$ to $10^{-6}$, for a spherical shell of inner radius 1/2 and outer radius 3/2. Extending Greenspan's analysis to a spherical shell, in the asymptotic limit this quantity should now be

$$i\lambda/E^{1/2} = \frac{(1+\rho^4)(1-\rho)}{1-\rho^5}(-2.620+0.259i),$$

where $\rho = r_i/r_o$ is the radius ratio. For $\rho = 1/3$ this yields

$$i\lambda/E^{1/2} = -1.776+0.176i.$$

The asymptotic decay factor is thus again in excellent agreement with the numerical values obtained here. The agreement in the asymptotic frequency correction is again not quite so good, presumably for the same reason as before.

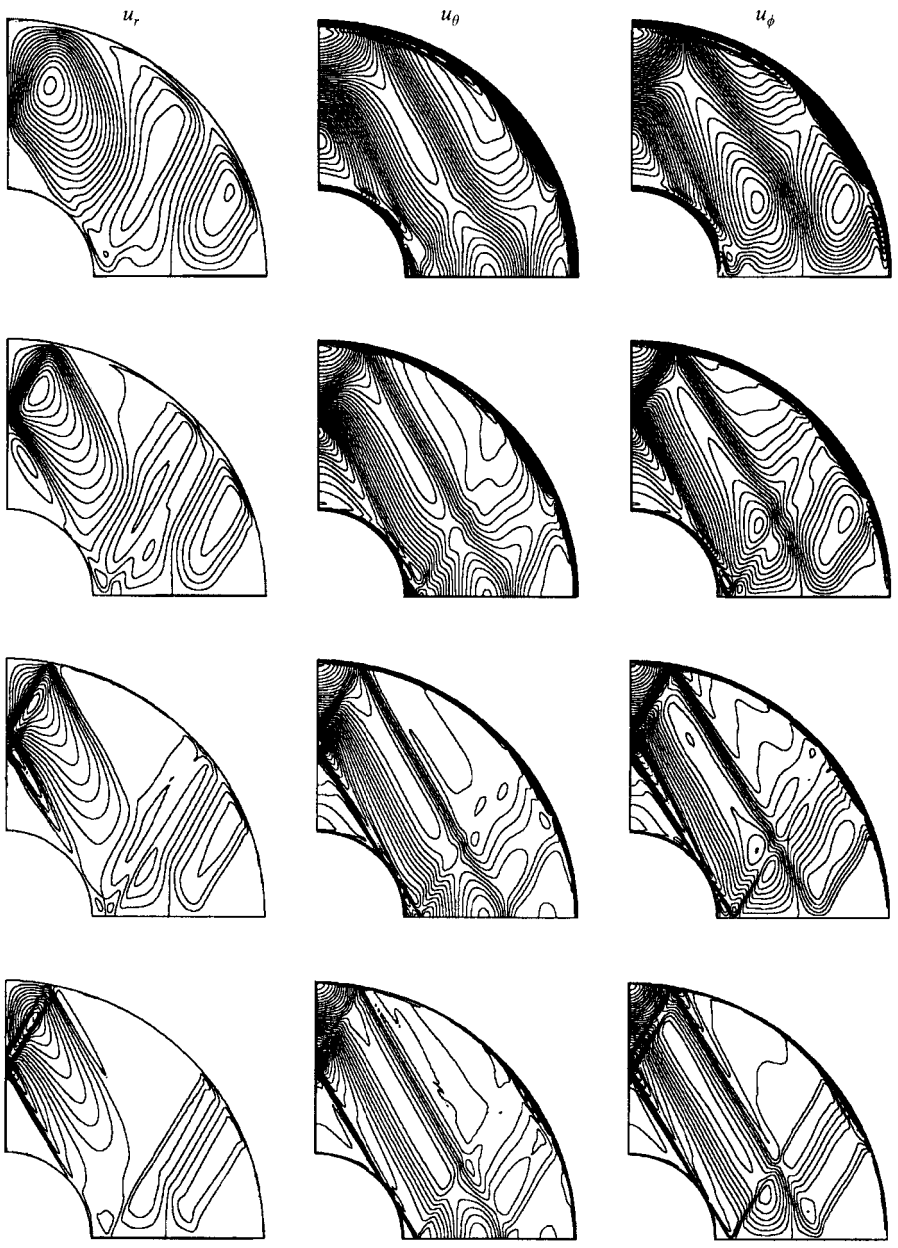


FIGURE 3. The structure of the spherical-shell eigenmodes $\boldsymbol{u}_0$. From top to bottom $E = 10^{-4}$, $10^{-4.5}$, $10^{-5}$, $10^{-5.5}$. Contour intervals of 0.02.

Turning again to the structure of the eigenmodes, figure 3 shows the solutions at $E = 10^{-4}$ to $10^{-5.5}$. The amplitude has been normalized as before, and the particular meridional sections have again been chosen to emphasize the structure of the shear layers. One notes again the internal shear layers, inclined at 30° to the axis of rotation. It is worth remarking that, for this particular frequency, this reflection pattern exactly closes on itself for all $\rho \leqslant 1/2$.

Of the three possible characteristic directions discussed in the introduction, only the one with the shear layer tangential to the inner Ekman layer eruption, and possibly also

the one with the shear layer non-tangential to the outer Ekman layer eruption, seem to be excited. The shear layer non-tangential to the inner Ekman layer eruption does not seem to be excited at all. This is presumably the result of the smoothing accomplished by the tangential shear layer, which effectively hides the inner boundary layer eruption.

Because the tangential shear layer is spawned by an $O(E^{2/5})$, as opposed to an $O(E^{1/5})$, generating region, it is indeed considerably thinner. The spherical-shell shear layer at $E = 10^{-5}$ is already thinner than the full-sphere shear layer at $E = 10^{-6}$. The precise scaling is again not inconsistent with the $O(E^{1/3})$ scaling derived in I. Also, one notes that the flow within the shear layers again decreases with decreasing $E$. Finally, it has been noted by Walton (1975) that such shear layers decay algebraically rather than exponentially at their edges. As a result, the flow within the shear layer reflection pattern is still strongly influenced by them, and hence the contours align with the characteristic directions.

## 4. Numerical solution of the nonlinear problem

As indicated in the introduction, the eigenmodes $\boldsymbol{u}_0$ of (1.7) will induce the axisymmetric nonlinear response

$$\frac{\partial}{\partial t}\boldsymbol{u}_1 + 2\hat{\boldsymbol{k}} \times \boldsymbol{u}_1 = -\nabla p + E\nabla^2 \boldsymbol{u}_1 + \boldsymbol{F}, \tag{4.1}$$

where $\boldsymbol{F}$ is the axisymmetric component of $-(\boldsymbol{u}_0 \cdot \nabla)\boldsymbol{u}_0$, and is known to have the particular time-dependence $\partial/\partial t \equiv -2\lambda_i$, which will therefore also be the time-dependence of $\boldsymbol{u}_1$. As in Hollerbach (1994*b*), we begin by decomposing:

$$\boldsymbol{u}_1 = v\hat{\boldsymbol{e}}_\phi + \nabla \times (\psi \hat{\boldsymbol{e}}_\phi). \tag{4.2}$$

The $\phi$-components of (4.1) and its curl then yield

$$2\frac{\partial \psi}{\partial z} + (2\lambda_i + E\,\mathrm{D}^2)\, v = -\boldsymbol{F}_\phi, \tag{4.3a}$$

$$2\frac{\partial v}{\partial z} - (2\lambda_i + E\,\mathrm{D}^2)\,\mathrm{D}^2 \psi = -(\nabla \times \boldsymbol{F})_\phi, \tag{4.3b}$$

where the operators

$$\frac{\partial}{\partial z} = \cos\theta \frac{\partial}{\partial r} - \frac{\sin\theta}{r}\frac{\partial}{\partial \theta}, \tag{4.4a}$$

$$\mathrm{D}^2 = \nabla^2 - (r\sin\theta)^{-2}. \tag{4.4b}$$

The solution of (4.3) is then a trivial modification of the solution presented in Hollerbach (1994*b*), the only difference being the inclusion of the $2\lambda_i$ terms. We again expand the angular structure of $v$ and $\psi$ in terms of $N_2$ associated Legendre functions, and as before the two operators $\partial/\partial z$ and $\mathrm{D}^2$ couple only adjacent modes. The radial structure is again collocated at $M_2$ Chebyshev collocation points (the details of the radial expansions are again slightly different for the full sphere and the spherical shell).

Because $\boldsymbol{F}$, being quadratic, has more structure than $\boldsymbol{u}_0$, one should take $N_2$ and $M_2$ to be greater than $N_1$ and $M_1$, ideally twice greater. But since $N_1$ and $M_1$ were already taken to be so large as to push the limits of the available computer memory, one cannot quite do so. However, since the block tri-diagonal matrix to be inverted is now real

rather than complex, one can increase $N_2$ and $M_2$ somewhat. Whereas for $N_1$ and $M_1$ we could only take $N_1 = M_1 = 100$, for $N_2$ and $M_2$ we can take $N_2 = M_2 = 135$.

## 5. Nonlinear results

### 5.1. *Full sphere*

Figure 4 shows the structure of the nonlinear response at $E = 10^{-5}$, $10^{-5.5}$, and $10^{-6}$. The top rows shows the azimuthal velocity $v$, the middle row shows the streamfunction $s\psi$, and the bottom row shows the axially averaged velocity $\bar{v} = z_o^{-1} \int_0^{z_o} v \, dz$ as a function of cylindrical radius $s$. The most noteworthy feature of the nonlinear response is this set of nested, differentially rotating cylinders evident in $v$ and $\bar{v}$. We believe these to be the cylindrical shear layers so evident in the experiments of Vanyo *et al.* (1995).

Because (5.4) is essentially independent of time ($2\lambda_i$ being small according to table 1), its characteristics are now cylinders instead of cones. Thus, even though the linear eigenmodes exhibit inclined oscillatory shear layers, the nonlinear responses exhibit axially aligned steady shear layers, which appear as cylinders parallel to the axis of rotation. Not surprisingly, the amplitude of these shear layers *within the* $\epsilon^2$ *scaling* increases with decreasing Ekman number, as it becomes increasingly easy to excite these geostrophic modes. Perhaps more surprisingly, the number of these shear layers also seems to increase with decreasing Ekman number. We unfortunately cannot achieve sufficiently small Ekman numbers to determine whether this increase in the number of oscillations in $\bar{v}$ persists indefinitely.

The most pronounced mean flow shear layers seem to occur at $s \to 0$ and at $s = \cos 30° = 0.86$. The strong shear layer at $s \approx 0.86$ is presumably caused by the sudden absence of the inclined oscillatory shear layers for $s > 0.86$, as noted in I. A similar shear layer in the mean flow was derived analytically by Busse (1968) to explain the original observations of Malkus (1968). Busse's asymptotic analysis considered the breakdown of the oscillatory Ekman layer at 30°, and the one mean flow shear layer it induces. We here consider not only the breakdown of the Ekman layer, but also the inclined oscillatory shear layers spawned thereby, and so we obtain more than one mean flow shear layer.

The rather strong shear layers at the axis $s \to 0$ are presumably caused by a geometrical focusing effect, whereby the inclined shear layers become concentrated in an increasingly small volume as they approach the axis. If, instead of the velocity $\bar{v}$, we had plotted the angular velocity $\bar{\omega} = \bar{v}/s$, which is presumably what is visualized in the experiments, these shear layers at the axis would have dominated the entire picture. There is some evidence for strong axial shear layers in the experiments of both Malkus (1968) and Vanyo *et al.* (1995). (Greenspan 1968, p. 175, also reproduces a photograph by Malkus.) Unfortunately, it is rather difficult to obtain quantitative information from the experiments about the relative strength of these various shear layers, preventing any precise comparison. One should also bear in mind that the experiments considered the precessionally forced mode in a spheroid, whereas we have considered the unforced mode in a sphere. Also, as noted in the introduction, the experiments are in the more strongly nonlinear regime, whereas we are only in the weakly nonlinear regime. Thus, there may well be subtle differences in the quantitative details. In any case, the presence of these axial shears is certainly a potential source of the instability observed in the experiments at sufficiently large precession rates.

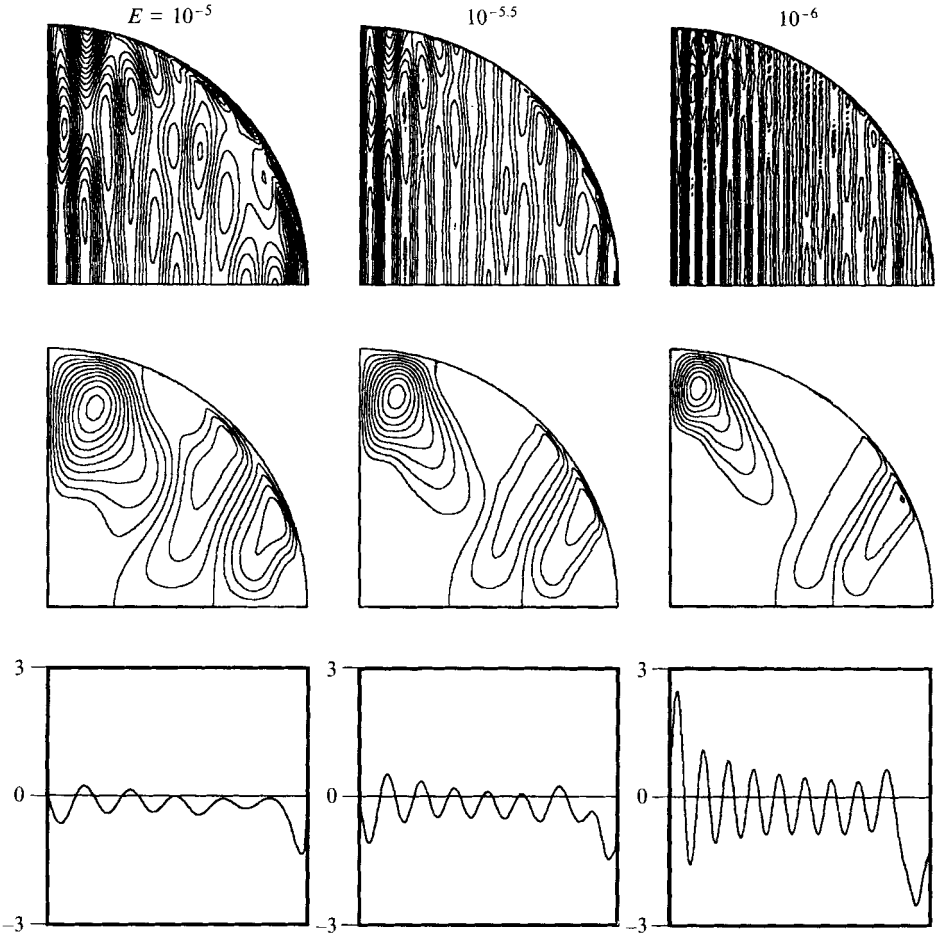


FIGURE 4. The structure of the nonlinear response $\boldsymbol{u}_1$ in the full sphere. From top to bottom the azimuthal velocity $v$, the streamfunction $s\psi$, and the axially averaged velocity $\bar{v}$.

### 5.2. *Spherical shell*

Figure 5 shows the structure of the nonlinear response in the spherical shell, at $E = 10^{-4}$, $10^{-4.5}$, and $10^{-5}$. One notes clearly the signature of the strong oscillatory shear layer tangential to the inner boundary layer eruption. The axially averaged velocity $\bar{v}$ displays all the features of the spherical case, albeit with less oscillations in the sign of the flow. Significantly, as in the spherical case, the number of these reversals in sign increases as the Ekman number decreases, and the last reversal in sign occurs precisely at the outer boundary eruption. This latter feature is not reproduced at the inner boundary eruption as the tangential shear layer spawned here propagates in both directions away from the eruption.

## 6. Conclusion

In this work we have considered a particular inertial oscillation of interest in rotating and precessing flows. We have demonstrated through a direct numerical solution that the Ekman layer associated with this spin-over mode does indeed change scalings at a certain critical latitude of 30° for this particular mode, as noted previously by Roberts

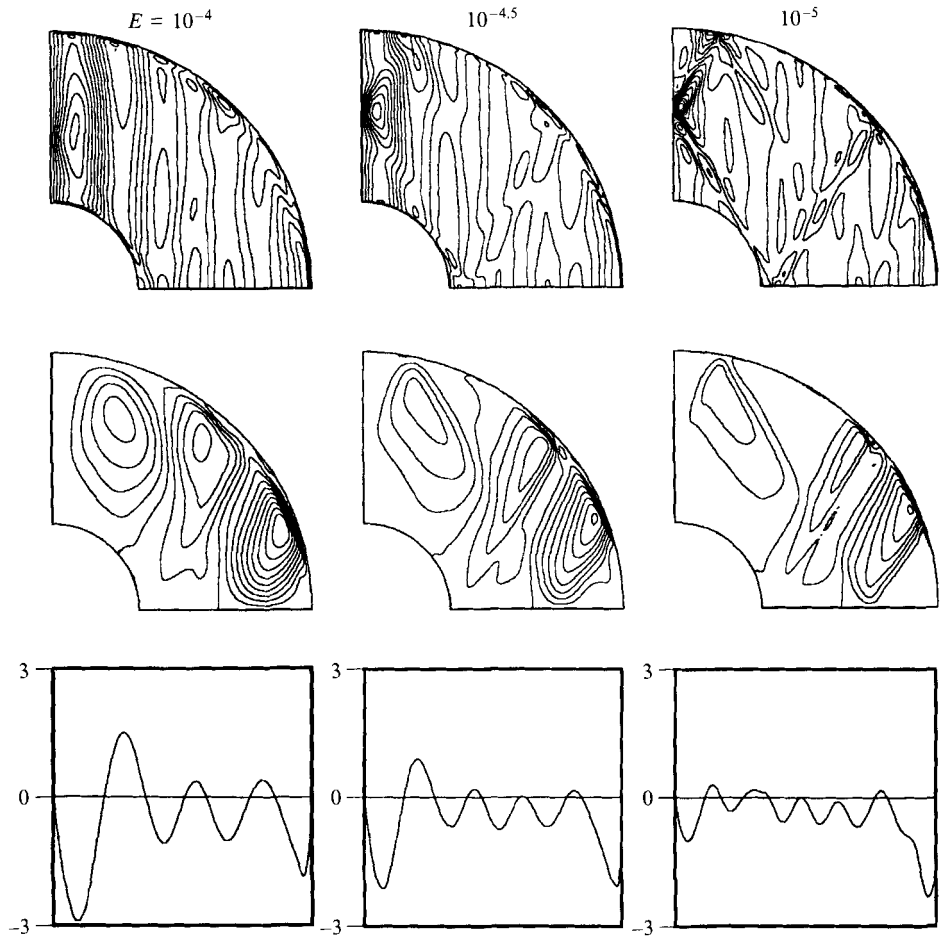


FIGURE 5. The structure of the nonlinear response $\boldsymbol{u}_1$ in the spherical shell. From top to bottom the azimuthal velocity $v$, the streamfunction $s\psi$, and the axially averaged velocity $\bar{v}$.

& Stewartson (1963). We have found that this local thickening of the boundary layer at the critical latitude gives rise to internal shear layers, which owing to their oscillatory nature propagate along characteristic directions inclined to the rotation axis. As a result, they penetrate throughout the interior of the fluid. Depending upon whether or not they are tangential to the boundary layer at the critical latitude, they see generating regions of different thicknesses, and this determines their scalings in the interior of the fluid. The existence of these shear layers, however, does not appear to affect the standard asymptotic result (Greenspan 1964) for the complex viscous frequency shift; we obtained agreement to within 1%. This confirms the general scaling arguments of Stewartson & Roberts (1963) that at lowest order the boundary layer eruptions are not important for the viscous frequency shifts.

We have also demonstrated that these oscillatory shear layers appear to have important consequences for the induced mean flow profile. In addition to the one mean flow shear layer at $s = 0.86$ previously obtained by Busse (1968), we also obtain others for $s < 0.86$, which appears to be in better agreement with the experimental results.

Finally, it should be emphasized that this numerical method is in no way restricted to this particular inertial oscillation. By choosing a different inviscid frequency, or a

different equatorial symmetry, or azimuthal wavenumber in (2.2), one can obtain other inertial oscillations. For example, axisymmetric inertial oscillations have been considered, both in a full sphere (Aldridge & Toomre 1969), as well as in a spherical shell (Aldridge 1972). By suitably modifying this code, it should be possible to investigate the shear layers associated with such modes as well.

## REFERENCES


ABRAMOWITZ, M. & STEGUN, I. A. 1968 *Handbook of Mathematical Functions*. Dover.

ALDRIDGE, K. D. 1972 Axisymmetric inertial oscillations of a fluid in a rotating spherical shell. *Mathematika* **19**, 163–168.

ALDRIDGE, K. D. & TOOMRE, A. 1969 Axisymmetric inertial oscillations of a fluid in a rotating spherical container. *J. Fluid Mech.* **37**, 307–323.

BUSSE, F. H. 1968 Steady fluid flow in a precessing spheroidal shell. *J. Fluid Mech.* **33**, 739–751.

FEARN, D. R. 1991 Eigensolutions of boundary value problems using inverse iteration. *J. Comput. Appl. Math.* **34**, 201–209.

GREENSPAN, H. P. 1964 On the transient motion of a contained rotating fluid. *J. Fluid Mech.* **21**, 673–696.

GREENSPAN, H. P. 1968 *The Theory of Rotating Fluids*. Cambridge University Press.

HOLLERBACH, R. 1994*a* Imposing a magnetic field across a nonaxisymmetric shear layer in a rotating spherical shell. *Phys. Fluids* **6**, 2540–2544.

HOLLERBACH, R. 1994*b* Magnetohydrodynamic Ekman and Stewartson layers in a rotating spherical shell. *Proc. R. Soc. Lond.* A **444**, 333–346.

KERSWELL, R. R. 1993 The instability of precessing flow. *Geophys. Astrophys. Fluid Dyn.* **72**, 107–144.

KERSWELL, R. R. 1995 On the internal shear layers spawned by the critical regions in oscillatory Ekman boundary layers. *J. Fluid Mech.* **298**, 311–325 (referred to herein as I).

MALKUS, W. V. R. 1968 Precession of the Earth as the cause of geomagnetism. *Science* **169**, 259–264.

PETERS, G. & WILKINSON, J. H. 1971 The calculation of specified eigenvectors by inverse iteration. *Handbook for Automatic Computation*, Vol. 2, pp. 418–439. Springer.

POINCARÉ, H. 1910 Sur la précession des corps déformables. *Bull. Astron.* **27**, 321–356.

ROBERTS, P. H. & STEWARTSON, K. 1963 On the stability of a Maclaurin spheroid of small viscosity. *Astrophys. J.* **137**, 777–790.

STEWARTSON, K. & ROBERTS, P. H. 1963 On the motion of a liquid in a spheroidal cavity of a precessing rigid body. *J. Fluid Mech.* **17**, 1–20.

VANYO, J. P., WILDE, P., CARDIN, P. & OLSON, P. 1995 Experiments on precessing flows in the Earth's liquid core. *Geophys. J. Intl* **121**, 136–142.

WALTON, I. C. 1975 Viscous shear layers in an oscillating rotating fluid. *Proc. R. Soc. Lond.* A **344**, 101–110.